Available online at www.sciencedirect.com
SCIENCE DIRECT®
International Journal of Heat and Fluid Flow 25 (2004) 91–102
International Journal of HEAT AND FLUID FLOW
www.elsevier.com/locate/ijhff

Dynamic surface tension measurements of molten Sn/Pb solder using oscillating slender elliptical jets

E.A. Howell [a], C.M. Megaridis [a,*], M. McNallan [b]

[a] Department of Mechanical and Industrial Engineering (M/C 251), University of Illinois at Chicago, 842 W. Taylor Street, Chicago, IL 60607-7022, USA
[b] Department of Civil and Materials Engineering, University of Illinois at Chicago, Chicago, IL 60607, USA

Received 6 July 2003; accepted 8 October 2003

Abstract

The present study investigates the *dynamic* surface tension of molten 63%Sn–37%Pb eutectic solder at timescales 1–3 ms applicable to solder jetting applications in microelectronics manufacturing. The oscillating jet method is employed to measure the surface tension of the melt when ejected into nitrogen atmospheres containing controlled amounts of oxygen from 15 ppm to 21% (mol). Typical jet ejection conditions correspond to $We = 0.16$, $Re = 49$, and $Fr = 165$. The molten solder is steadily forced through an elliptical capillary (aspect ratio of ~2), thus forming a *stationary* oscillating jet. The shape evolution of the jet is affected by the liquid/gas interface properties and is used, along with an existing theoretical model, to determine the surface tension of the liquid metal as a function of distance (likewise, surface age) from the orifice. The experimental data reveals dynamic surface tension behavior at 3700 ppm O_2 concentration, and indicates a characteristic time below 1 ms for the molten-metal surface to be saturated by adsorbed oxygen at ambient O_2 concentrations of 1% or higher. Mass diffusion in the gas phase is found to be the rate limiting process controlling oxygen adsorption on the solder melt surface. The results provide crucial information needed to reduce solder surface degradation, which hampers the successful implementation of solder jetting technology.

Keywords: Dynamic surface tension; Molten Sn/Pb solder; Capillary jet; Oxygen adsorption; Solder jetting

1. Introduction

Solder jetting technology (Hayes et al., 1993) is evaluated for use in high-density electronics assembly applications where solder is employed as an attachment and/or structural material for mounting of electronic components to substrates. This technology relies on inkjet printing principles to create and place monodisperse arrays of molten solder droplets of approximately 30–120 μm diameter on electronic substrates/components at rates up to 1000 per second. The droplets solidify after impact, thus forming bump deposits, which are subsequently used for the flip-chip bonding of electronic components to the substrate. A primary advantage of this technique is that no leads are required. Furthermore, inkjet based solder deposition requires no tooling, and is low-cost (no masks or screens are required), non-contact, flexible, easily automated using digital technology, suitable for a manufacturing environment (does not operate in a vacuum like liquid metal ion systems), highly repeatable, as well as high resolution (positioning capability better than 10 μm). Due to the above reasons, solder jetting technology has the potential to enable critical improvements in small, lightweight packages and other electronic products (Godin, 1996).

Even though solder jetting technology has shown promise to achieve solder deposition at pitch geometries well below what is feasible with stencil printing and at costs substantially below plating and vacuum techniques, there exist a few formidable challenges which must be overcome before further advancement. Because maximum throughput is an important requirement in electronic assembly, solder jetting is performed *openly* but with local environment control. A sheathing nitrogen

* Corresponding author. Tel.: +1-312-996-3436; fax: +1-312-413-0447.
E-mail address: cmm@uic.edu (C.M. Megaridis).

0142-727X/$ - see front matter © 2003 Elsevier Inc. All rights reserved.
doi:10.1016/j.ijheatfluidflow.2003.10.003

ring flow surrounds the solder jet to minimize contact of the melt with oxygen, which can drastically delay the jet atomization through reduction of surface tension (Wallace, 1993) and degrade the effective adherence of the solder deposits to the targets. Furthermore, jetting on non-flat (3-dimensional) substrates makes it even more challenging to eliminate contact with oxygen and achieve targeting accuracy. Thus, a major development challenge in the commercialization of solder jetting technology stems from the need to maintain adequate control of the local environment around the atomizing fluid and the formed droplets under a wide variety of operating conditions. To this end, the limitations of solder jetting must be quantified as a function of oxygen content in the local inert environment.

Surface tension and its critical influence on droplet formation are of central importance in solder jetting. Due to the high reactivity of many liquid metals, the presence of surface active elements—even in trace concentrations in the local atmosphere—degrades interface tension σ (Keene, 1988), which, in turn, compromises the effectiveness of the jetting process. Tin-containing melts are especially susceptible to surface degradation caused by oxygen adsorption (Passerone et al., 1990). Due to the ubiquitous presence of oxygen in the atmosphere, measurements of surface tension of metal melts exposed to O_2 are needed to assist the commercialization of solder jet technology or other relevant technologies. It is important to note, however, that the time scales in jet capillary breakup are typically of the order of a few milliseconds, thus requiring time resolution near or below a millisecond. This severe requirement eliminates most standard methods for dynamic surface tension measurement. Jet instability techniques have been used with success to determine interfacial tension of aqueous solutions in inkjet printing technology (Ronay, 1978a). More recently, Bellizia et al. (2003) utilized a capillary jet instability method to document the evolution of axisymmetric solder jet swells and necks, which was translated into the variation of molten solder surface tension at surface ages between 2 and 4 ms from the exit orifice. Using capillary jet instability techniques and low melting point metals, one can estimate the surface tension of newly formed surfaces within a time window of a few ms after formation, i.e., during the early period when surface properties have not been fully compromised by adsorbed oxygen.

There are several additional experimental techniques capable of measuring surface tension of molten metals at the time scales of interest. These include the oscillating jet (Bechtel et al., 1995), oscillating droplet (Hiller and Kowalewski, 1989) and excited jet (Ronay, 1978b) techniques, which are capable of producing surface tension measurements at surface ages <3 ms, a requirement imposed by the solder jetting velocity ($\sim$1 m/s) and the printhead-to-substrate distance ($\sim$5 mm). The above techniques can produce dynamic surface tension data, which is important when the surface tension of Sn/Pb solder rapidly decays upon exposure to adequate O_2 concentrations in the surrounding atmosphere.

The oscillating jet technique is used in this study in conjunction with the theoretical model of Bechtel et al. (1995) to convert molten Sn–Pb solder jet standing waveforms to surface tension values. Measurements are performed for six different oxygen concentrations ranging from 15 ppm to 2.03% (balance N_2), as well as in air. The dynamic surface tension of the eutectic melt, which is jetted through an elliptical orifice into these controlled atmospheres, is measured at surface ages 1–3 ms. The documented decay of surface tension is interrogated with respect to the formation of an adsorbed oxygen monolayer on the exposed surface of the melt. Finally, the time scales of oxygen adsorption from the surrounding gas onto the solder jet interface are estimated and compared to a simple theoretical model.

2. Theoretical background

When a liquid is forced through an elliptical orifice, it produces a standing, oscillating jet, whose cross section changes with distance from the orifice (Rayleigh, 1890). The elliptical jet is driven by the restoring action of surface tension as it deforms to attain a circular shape downstream (Bechtel et al., 1995). However, due to momentum produced by surface forces, the jet overshoots the preferred circular shape and produces an elliptical cross section, having major and minor axes reversed from the original configuration. This alternating process continues for several wavelengths downstream until the oscillations die out or the jet atomizes. The main advantage of this technique is that it produces a *stationary* jet for the entire length before breakup occurs. The stationary shape allows high-quality measurement of jet features (amplitude and wavelength), which can be used to deduce values of fluid properties as a function of distance from the orifice (likewise surface age).

The idea of using oscillating jets to measure surface tension began in the 19th century with Rayleigh (Rayleigh, 1879; Rayleigh, 1890). Rayleigh produced the first mathematical description of an oscillating jet issued from an elliptical orifice, and used his model to perform surface tension measurements on water. Rayleigh's work on the oscillating jet created a new and superior method of surface tension measurements.

Bohr (1909) understood the inherent benefit of Rayleigh's discovery. However, Rayleigh's model assumed

the shape of the jet did not deviate much from a circular cylinder, and did not account for viscosity. Bohr added the effects of viscosity, and allowed for finite amplitudes in his improved model. It should be noted that while Bohr's work was published in 1909, this model still finds use today (Shavit and Chigier, 1995). Correction factors and various modifications have been made (see references cited in Bechtel et al., 1995), but the basic theory remains the same.

Bechtel et al. (1995) developed an integro-differential model to determine dynamic surface tension of a newly formed surface issued from an elliptical orifice. This model consists of a system of dimensionless, non-linear, integro-differential equations, which cannot be explicitly solved for jet shape or material properties (surface tension or viscosity). The model accounts for gravity acting in the direction of jet propagation, and allows surface tension and viscosity to be variable with respect to distance from the orifice, i.e., time. In addition, while Bohr modified Rayleigh's model to allow for viscosity and finite amplitudes, producing an ad hoc solution, Bechtel et al. accounted for these effects in a three-dimensional geometry. The details of the model can be found in Bechtel et al. (1995). For completeness, the model equations, assumptions and definitions are presented briefly in the following.

The basic assumptions considered by Bechtel et al. (1995) are:

- The jet is slender, in terms of the slenderness ratio ε, i.e., $0 < \varepsilon \ll 1$. The slenderness ratio is defined as $\varepsilon = r_0/z_0$, where r_0 is the characteristic radius, and z_0 is the characteristic length in the axial direction z. For a specific wavelength, the characteristic radius is taken as $r_0 = (R_{\mathrm{B,max}} R_{\mathrm{B,min}})^{1/2}$, where $R_{\mathrm{B,max}}$ and $R_{\mathrm{B,min}}$ are the major and minor semiaxes, respectively, at the beginning of the wavelength. The wavelength offers a reasonable estimate of the characteristic length z_0.
- The flow is steady.
- The fluid is viscous, but not necessarily Newtonian.
- The fluid density is constant along the wavelength over which measurements are performed. The surface tension and viscosity may change along this length.
- The jet exits the elliptical orifice with its cross section remaining elliptical (although with varying semiaxes) for the distance over which measurements are taken. Bechtel et al. (1995) presented experimental and numerical evidence that for moderate eccentricities (2.5:1 or less) the jet shape remains nearly elliptical at least for a few wavelengths of oscillation.

The equations describing the shape evolution of the jet along the longitudinal direction z are

$$\left[1+\phi_1^4\left(\frac{2z}{Fr}+1\right)\right]\frac{\mathrm{d}^2\phi_1}{\mathrm{d}z^2}-\frac{2\left(\frac{\mathrm{d}\phi_1}{\mathrm{d}z}\right)^2}{\phi_1}+\frac{4}{We}\phi_1^3(\kappa_s-\kappa_c)+\frac{1}{Fr}\left[\phi_1^4-\left(\frac{2z}{Fr}+1\right)^{-1}\right]\frac{\mathrm{d}\phi_1}{\mathrm{d}z}-\frac{2}{Fr^2}\left(\frac{2z}{Fr}+1\right)^{-2}\phi_1+\frac{48}{Re}\left(\frac{2z}{Fr}+1\right)^{-\frac{1}{2}}\phi_1^2\left[\left(\frac{2z}{Fr}+1\right)\frac{\mathrm{d}\phi_1}{\mathrm{d}z}+\frac{\phi_1}{2Fr}\right]=0 \tag{1}$$

$$\phi_2(z)=\frac{1}{\upsilon(z)\phi_1(z)} \tag{2}$$

$$\upsilon(z)=\left(\frac{2z}{Fr}+1\right)^{\frac{1}{2}} \tag{3}$$

where ϕ_1 and ϕ_2 are, respectively, the major and minor jet semiaxes (normalized with respect to r_0), while υ denotes the component of fluid velocity along the jet propagation axis. ϕ_1, ϕ_2 and υ all vary with z. The Weber, Reynolds, Froude numbers and the $(\kappa_s-\kappa_c)$ term found in Eqs. (1)–(3) are defined, respectively, as

$$We=\frac{\rho r_0^3\upsilon_0^2}{\sigma(z)z_0^2},\quad Re=\frac{\rho\upsilon_0 r_0^2}{\eta(z)z_0},\quad Fr=\frac{\upsilon_0^2}{gz_0} \tag{4}$$

$$\kappa_s-\kappa_c=\frac{1}{\pi}\left(\frac{2z}{Fr}+1\right)^{-\frac{1}{2}}\times\int_0^{2\pi}\frac{(\cos^2\theta-\sin^2\theta)\mathrm{d}\theta}{\left[\phi_1^2\sin^2\theta+\phi_1^{-2}\left(\frac{2z}{Fr}+1\right)^{-1}\cos^2\theta\right]^{\frac{3}{2}}} \tag{5}$$

In the above expressions, surface tension, density and elongational viscosity are denoted by σ, ρ and η, respectively. In the formulation of Bechtel et al. (1995), σ and η are allowed to change along z, therefore, the values of *We* and *Re* appearing in Eq. (1) also vary with z. g is the acceleration of gravity. The characteristic velocity υ_0 is the axial velocity at the beginning of the wavelength, and can be calculated from the flow rate and the known orifice cross sectional area. The dimensionless jet profile is defined in terms of the values of ϕ_1 and ϕ_2 along z. The direct problem, as defined by Bechtel et al. (1995), involves the calculation of the jet waveform, i.e., $\phi_1(z)$ and $\phi_2(z)$, for specified surface tension and viscosity functions of z, and certain conditions at $z=0$ (flow rate and orifice geometry). The inverse problem involves the determination of fluid surface tension and viscosity to match a specified jet profile, as determined from experimental measurements. In the present study, the adopted formulation of the inverse problem is based on the assumption that surface tension and viscosity are constant in the same wavelength, although σ is allowed to change between wavelengths, thus producing $\sigma(z)$ information. The

formulation of Bechtel et al. (1995) was extended in Bechtel et al. (1998), where σ was allowed to vary within a wavelength. The functional variations of σ represented three different surface tension decay forms taken from the literature.

3. Experimental

3.1. Fluid properties

The solder used in this investigation is a high-purity eutectic alloy of tin and lead (63%Sn–37%Pb) produced by Witmetaal (a company of the Cookson Group). This low melting point material (183 °C) is used for electronic components, such as computers and communications equipment, where only moderate heat exposure can be tolerated by the delicate components. The solder is packaged in pellet form and shipped in sealed aluminum bags containing nitrogen gas to minimize oxidation of the solder pellets prior to use. Table 1 shows the material mass composition analysis, as provided by the manufacturer.

3.2. Microjet printhead

The primary component of the experimental apparatus was the MicroJet printhead (see Fig. 1), which utilized a custom jetting device. The purpose of the printhead was to liquify the solder pellets, provide a reservoir for the molten solder, and produce the oscillating solder jet. The printhead contained a cylindrical stainless steel reservoir with an inner diameter of 27 mm and an inner height of 79 mm. The top of the reservoir was a screw-on cap with a nitrogen gas inlet for backpressure. The bottom of the reservoir had a mating attachment to accept the jetting device. The reservoir interior walls were treated by a passivation process, which formed a stable oxide layer, thus preventing the solder from being contaminated by forming intermetallics. Heat for the MicroJet printhead was supplied by two stick heaters (Watlow), each connected to a controller (Omega). Thermocouples were installed to monitor temperature and provide active input for the heater controllers.

Table 1
Material mass composition analysis for 63Sn/37Pb solder

Sn	63.41	Ni	$\leqslant 0.001$
Sb	0.009	Bi	0.006
Pb	Balance	Cd	$\leqslant 0.001$
Cu	0.001	Ag	$\leqslant 0.001$
Zn	$\leqslant 0.001$	Al	$\leqslant 0.001$
Fe	$\leqslant 0.001$	In	0.002
As	$\leqslant 0.001$		

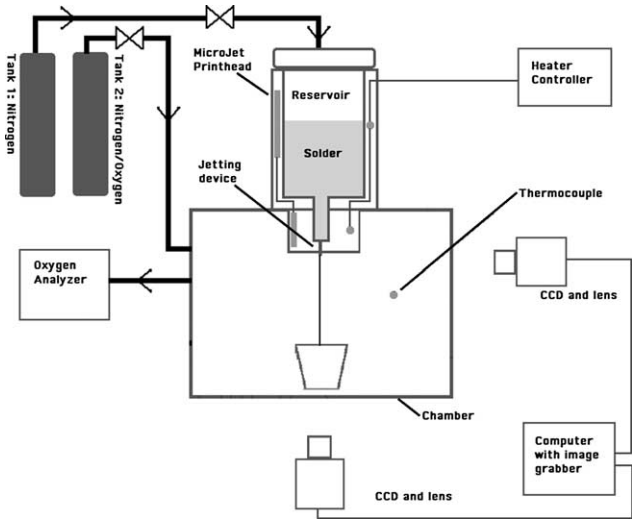

Fig. 1. Experimental apparatus schematic.

The custom jetting device consisted of an elliptical stainless steel capillary, which was mounted in a casing with identical external dimensions as the standard MicroJet jetting device. The casing allowed for the custom elliptical jetting device to directly mate with the MicroJet printhead. The elliptical capillary was formed from a 22-gauge hypodermic stainless steel capillary with a length of 10 mm. The two ends of the capillary were polished to provide sharp, clean edges. Finally, a ~3 mm long end section of the overall 10 mm capillary length was pressed to attain an elliptical shape. The produced elliptical nozzle had a major axis of 664 μm and a minor axis of 312 μm (inner dimensions, as measured optically). Thus, the characteristic jet radius upon emergence from the orifice is $r_0 = 228$ μm. Typical jet wavelengths were of the order of 2 mm, thus resulting in a slenderness ratio $\varepsilon = 0.11$ (slender jet). The elliptical capillary and the casing components were also treated through the same passivation process as the reservoir. All components were finally assembled and secured together using a high-temperature epoxy, which did not come into contact with the jetted fluid.

3.3. Environmental chamber

In order to control the N_2/O_2 gas mixture to which the solder melt was exposed, a rectangular environmental chamber was constructed of aluminum measuring 220 mm (W) × 220 mm (H) × 250 mm (L). Three glass windows on three vertical walls were used for visualization of the solder jet. The fourth vertical wall contained all electrical and gas ports, as well as the lighting for the side-view camera. The printhead was mounted on the lid of the chamber, with its lower portion protruding through the lid via a sealed fitting (see Fig. 1). A gas inlet provided the desired N_2/O_2 mixture to fill and purge the chamber. A gas outlet fed the chamber gas to

an oxygen analyzer (AMETEK Thermox TM-1B/2B). The calibrated analyzer gave an accurate (within 5% above 1 ppm), real time measurement of the oxygen concentration in the environmental chamber. An analog pressure gauge provided chamber pressure readings. A type-K thermocouple was installed to monitor the chamber temperature. The environmental chamber was mounted on a breadboard (TMC). External vibrations on the experimental apparatus were reduced by placing four sorbothane polymer bumpers (57% absorption efficiency, 70% specific damping) between the breadboard and the table.

3.4. Flow control and measurement equipment

Gas was supplied to the apparatus from two tanks (Fig. 1). Tank 1 contained pure N_2 gas and supplied backpressure to the printhead reservoir. An on/off valve and a regulator on Tank 1 was used for backpressure control. An in-line pressure transducer provided a readout of backpressure. The N_2/O_2 gas mixture for the environmental chamber was supplied by a second tank (Tank 2 in Fig. 1). A needle valve controlled the flow of the N_2/O_2 mixture gas into the chamber.

Inside the chamber, a mass flux measurement system was designed for the jetted material. The system was operated by recording the time it took for a given amount of liquid solder to accumulate into an initially empty retaining cup. The system included three separate stainless steel cups used for mass measurements during a run. To avoid buildup of tall solder structures, the retaining cups were heated to keep the solder in a molten state for the duration of the experiment. The cups were mounted on a rotating disk. A stepper motor and belt-drive mechanism allowed remote rotation of the disk, which was turned by 120° each time, to align a new cup with the jet. A digital scale with 0.1 mg accuracy was used for the jetted fluid mass measurements. Typical solder mass flow rates were 2.4 g/s, translating into average exit velocities of 1.8 m/s.

3.5. Visualization

The theoretical model requires two orthogonal views of the molten solder jet, one along each principal axis of the elliptical cross section. The two images were acquired using two CCD cameras outfitted with microscope lenses. Both cameras produced 640 (H) × 480 (V) pixel images and utilized identical macrovideo zoom lenses (Optem, 18–108 mm, f/2.5) with a minimum working distance of 140 mm. Each camera was mounted to the breadboard via a 3-axis translation stage for accurate positioning.

The jet images were captured using a image grabber board (Scion CG-7) installed in a personal computer. The standard resolution of the image grabber was identical to that of the cameras (640 × 480 pixels). The digitizer routed the video image directly to a video card (ATI Rage Orion), bypassing the computer processor, and allowing for real time viewing on the computer display. The images were processed using a combination of NIH Image and GraphicConverter software applications.

The view field of each camera was back-lit by an in-line array of 5 high-brightness blue LEDs (Panasonic, 15° viewing angle). A glass diffuser lens was positioned between the LED array and the solder jet in order to produce uniform backlighting. The LED array was driven by a pulse generator (HP 8013B, 10 V maximum output). This LED/pulse generator combination provided high-speed strobing ability, which was very useful for troubleshooting. However, the strobing feature was not needed during normal operation due to the stationary character of the jet.

3.6. Experimental procedure

First, the reservoir was filled with solder pellets using extreme care to minimize contamination of the solder during handling. The reservoir cap was then secured into place. The imaging system was adjusted in terms of position, focus, working distance, magnification, and aperture. The image-grabbing software was launched, producing a live video image of the nozzle. The heater controllers for the printhead were set and activated to a temperature of 175 °C using a ramp time of 30 min. The heaters for the solder retention cups were also activated. When the printhead temperature reached 100 °C, the chamber gas purging began. The chamber purging process consisted of flowing a prescribed N_2/O_2 mixture through the chamber initially at a relatively high velocity (chamber pressure was maintained at ~0.3–0.6 psig). When the printhead temperature reached 175 °C, the flow rate of the purging gas was reduced to obtain a chamber pressure of ~0.16 psig. The printhead heater controllers were set to 240 °C. The live video image was closely monitored for observing liquid flow from the nozzle orifice. Molten solder typically began dripping from the nozzle orifice when the printhead temperature reached ~210 °C. However, backpressure was not applied at that point, as it was estimated that not all of the solder was molten yet. Dripping of solder was slow and would generally stop within 30 s from starting. Typically, between 230 and 240 °C the molten solder would again commence dripping from the nozzle at a faster rate than before. At this point, backpressure was applied to the melt, thus producing an oscillating jet. The melt temperature influenced solder mass flux when the backpressure remained constant. For a given backpressure, the mass flux was measured to be higher at higher melt temperatures, and vice versa. This was attributed to the lower viscosity of the melt at higher temperatures. It

is noted that sometimes the solder did not stop dripping after the printhead first reached ~210 °C, and thus the experiment had to be conducted at this lower temperature. Approximately six sets of images were captured and stored in each case. The time (for mass flux measurements), chamber pressure, chamber temperature, printhead temperature, and chamber O_2 concentration were recorded. When jetting ceased (solder reservoir emptied), the heaters were switched off, all gas flows were terminated, and the captured set of images was saved for post processing. All primary components of the apparatus were then thoroughly cleaned for the next experiment.

3.7. Image processing

Image calibration was performed first to convert pixel measurements to physical lengths (in micrometers). Each digital image was enhanced by applying an "edge sharpening" algorithm. This procedure increased the contrast between the jet edge and its background. The major and minor semiaxes of the jet were then measured. Next, an "edge locating" algorithm defined the outline of the jet (see Fig. 2). The jet outline image was subsequently used to measure jet wavelengths and to estimate surface age along each wavelength on the image. Surface age over a specific wavelength was designated as that corresponding to the middle of this wavelength (see Fig. 2). It is worth noting that the dimensions of the solder jet at the orifice exit in Fig. 2 are ~630 and ~345 μm, which are slightly different than the corresponding principal dimensions of the elliptical orifice (664 and 312 μm, respectively).

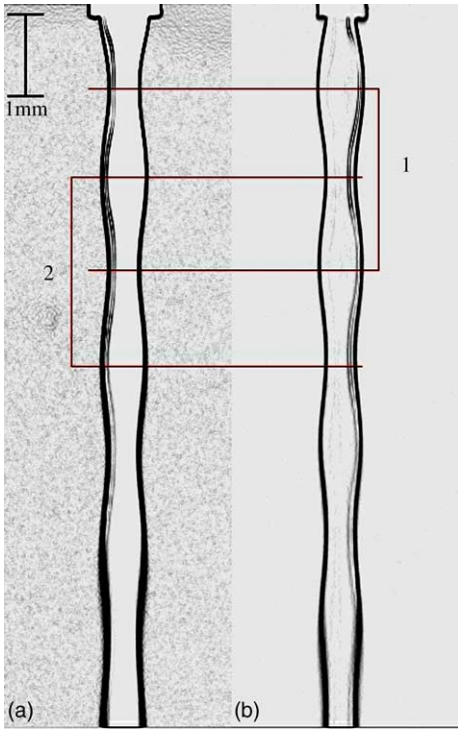

Fig. 2. Orthogonal views along the directions of the principal axes of an elliptical solder jet exposed to an atmosphere of 15 ppm O_2 (in N_2): (a) front view, (b) side view. The first two wavelengths (1 and 2), where surface tension measurements are performed, are indicated. The rectangular detail at the top of each image indicates the outline of the elliptical orifice. The length scale on the top left applies to both images.

4. Data analysis

The jet waveforms recorded in the experiments were utilized in conjunction with Eqs. (1)–(5) to deduce the variation of surface tension of the solder melt with distance from the orifice in different O_2/N_2 gas atmospheres. In this process, the liquid elongational viscosity η was considered to be constant throughout, and equal to three times the shear viscosity (fluid is Newtonian). The constant viscosity assumption is valid at low oxygen gas concentrations, as these do not affect bulk liquid viscosity. However, when the molten solder surface gets completely saturated by oxygen, the formation of a thin oxide layer may render this assumption invalid (Haj-Hariri and Poulikakos, 2000). The value of σ was assumed to be constant within the same wavelength; however, σ was allowed to vary between successive wavelengths. Consequently, the surface tension coefficient as a function of axial distance from the orifice $\sigma(z)$ was determined in terms of a set of discrete values (one point per wavelength) along the oscillating jet. Fig. 2 shows two orthogonal views of a solder jet in 15 ppm O_2 (in N_2) and demonstrates the concept of using successive wavelengths to deduce dynamic surface tension measurements. Discrete values of σ are calculated for the partially overlapping wavelengths 1, 2, and so on. The surface age, corresponding to the value of σ for a given wavelength, is determined using the distance from the orifice to the midpoint of the wavelength combined with the axial velocity of the jet. It is noted that the effect of gravity in determining surface age is not significant, as the measured distance is quite small (several mm) and the exit velocity is ~O(1 m/s). This translates into a practically constant value of velocity along z, i.e., $v(z) = v_0$. The value of v_0 was determined for each case by dividing the measured mass flow rate (Section 3.4), by the product of density and cross sectional area of the jet emerging from the orifice.

Assuming constant—albeit unknown—σ and constant η within each wavelength, the solution of the inverse problem in the current work featured an iterative numerical scheme. The model inputs are density, viscosity, mass flux, major and minor semiaxes at the beginning of the wavelength, and an estimate of the Weber number in the absence of the exact surface tension value. The model determines the jet shape,

i.e., $\phi_1(z)$, $\phi_2(z)$ and λ, that conforms to the input data. To find the actual Weber number (and thus, surface tension; see Eq. (4)) over a specific wavelength, the model iterates by altering the Weber number until the calculated wavelength equals the measured value. The surface tension coefficient σ for that particular wavelength is determined from the final value of *We*. It is noted that to terminate the iterations, the model seeks only matching of the wavelength λ, because σ primarily affects the wavelength, while viscosity mainly influences the amplitude of oscillations (Bechtel et al., 1995).

5. Experimental error in σ

Because in this investigation the surface tension was determined through the numerical solution of a set of integro-differential equations, an uncertainty analysis could not be readily applied using these equations. Instead, an implicit uncertainty analysis was performed in the following manner. First, the errors associated with the measurement of certain experimental parameters were estimated. These experimental parameters included mass flux, major and minor jet semiaxes, and wavelength. For mass flux, the estimated error was ±2% (combined error in solder weight and time). The measurement of major and minor semiaxes was within ±0.5 pixel, or ±7 μm. The corresponding error in measuring the major and minor semiaxes was ±3% and ±4%, respectively. Although the major and minor semiaxes were measured quite accurately due to the sharp contrast between the jet and the background, the wavelength was more difficult to measure. Unlike the semiaxes, there were no sharp edges to discern the wavelength in an accurate manner. The corresponding error in λ was estimated as ±3 pixels (±42 μm), which translated into a possible wavelength deviation of ±2%. The effect on surface tension from the individual sources identified above was determined by using a sample set of data, altering only one source of error (at maximum deviation) at a time, and running the computer code to obtain the new value of σ. The maximum error in mass flux resulted in a ±4% error in the surface tension calculation. For the major and minor semiaxes, the maximum deviation produced a ±1% and ±2% error, respectively, in the surface tension calculation. A maximum deviation in wavelength yielded a ±4% error in the surface tension calculation. Clearly, errors in measuring mass flux and wavelength had the largest influence on surface tension.

There were additional sources of error, which could not be included in this uncertainty analysis. One such error was the geometry of the nozzle cross section at the orifice. It was not possible to manufacture a nozzle with a perfectly elliptical cross section at the dimensions required by this experiment. While the nozzle cross section was elliptical in shape, it did not conform exactly to a mathematical ellipse. Another error source was the model assumption that the surface tension was constant over one wavelength. This introduced an error in the surface tension calculation when solder was jetted in certain O_2 concentrations, in which surface tension decreased rapidly.

6. Method validation using a test liquid

Before conducting experiments with molten solder, measurements were performed using deionized water. Fig. 3 displays the front and side images of an oscillating water jet; these images were used for surface tension calculations. While the jet in Fig. 3 is shown in a horizontal orientation, the actual jet was vertical during the experiment. The known value of surface tension of water at 20 °C is 72.8 mN/m (Munson et al., 2002). The surface tension from the water experiment was 76.5 mN/m, within 5% of the known value. The experimental value was obtained by averaging the data from the same experiment performed several times keeping the conditions unchanged. An interesting observation in the water experiments was that the calculated values of surface tension were consistently higher than the known value. The same observation was made by Reichard et al. (1997) who used the same technique to determine surface tension of mixtures of ethanol and distilled water. As a consequence, it is expected that this trend would also occur in the molten solder experiments.

7. Results for 63Sn–37Pb solder

Table 2 lists the solder surface tension coefficients at surface ages in the range 1–3 ms. These values were determined by exposing molten solder jets to different

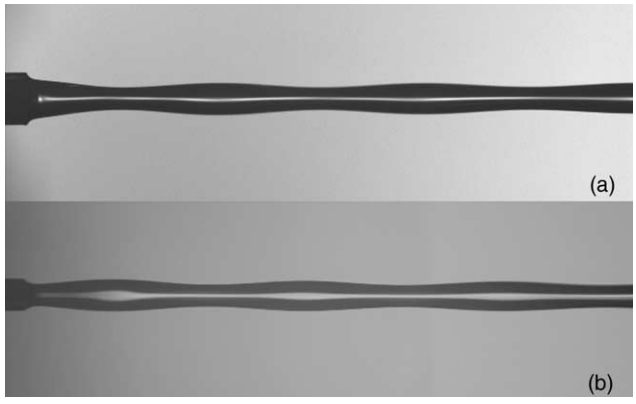

Fig. 3. Oscillating water jet: (a) front view, (b) side view. The actual orientation of the jet during the experiment was in the vertical direction.

Table 2
Surface tension (in N/m) of 63Sn–37Pb solder jetted in O_2/N_2 gas mixtures

Surface age (±0.1) (ms)	O_2 concentration (vol.) in N_2					
	15 ppm	103 ppm	990 ppm	3700 ppm	1.16%	2.03%
1	0.534	0.532	0.548	0.49	0.387	0.385
1.6	0.518	0.515	0.54	0.40	0.385	0.392
2.1	0.518	–	0.536	–	–	–
2.5	–	–	0.526	–	–	–

O_2/N_2 mixture atmospheres (compositions indicated in top row of this table). Each listed value of σ was determined as an average of several measurements performed under identical operating conditions. The values $\rho = 8218$ kg/m^3 and $\eta = 7.86 \times 10^{-3}$ kg/m s were used for liquid solder (Xiong et al., 1998). Using these properties, along with the definitions of Eq. (4) and the values $\sigma = 0.5$ N/m, $z_0 = 2$ mm, $r_0 = 228$ μm, and $v_0 = 1.8$ m/s, we obtain the typical values of $We = 0.16$, $Re = 49$, and $Fr = 165$. The melt temperature in all cases was in the range 210–245 °C (see Section 3.6), while the gas in the environmental chamber was at 45 °C. The missing values of σ in Table 2 at advance surface ages (i.e., axial locations further from the orifice) are due to poor definition of the jet shape away from the orifice. This is because the jet shape was more stable closer to the orifice, but became gradually less well defined downstream, thus making measurements there not possible.

For the three lower O_2 concentrations in Table 2, namely, 15, 103 and 990 ppm, the calculated σ at a surface age of 1 ms was slightly higher than the two subsequent values at 1.6 and 2.1 ms, although the surface tension was practically constant under the given timescale conditions. This common trend in all experiments with the lower O_2 concentrations may be indicative of residual nozzle influences on the oscillation of the molten solder jet (i.e., at 1 ms not enough time had elapsed to damp out all the effects of the nozzle). This same trend was also observed in experiments performed with deionized water. For the above reason, while the reported value of σ at 1 ms is considered to be reasonably accurate for the low O_2 concentrations, the corresponding values at 1.6 or 2.1 ms are believed to be more precise. Values of σ for the first wavelength of the oscillating jet (beginning at the nozzle orifice) are not reported herein because these results showed little reproducibility. It is believed that velocity relaxation events upon emergence from the nozzle were responsible for these discrepancies. Wavelength measurements began at one wavelength from the orifice (wavelength 1 of Fig. 2).

As stated above, the values of σ in Table 2 for O_2 concentrations 15, 103 and 990 ppm are essentially identical. Apparently these gas mixtures did not contain enough O_2 to reduce the surface tension of the melt within the <3 ms window available under the present operating conditions. Consequently, the results for these concentrations could be viewed as corresponding to those of pure (non-oxidized) 63Sn–37Pb solder. The calculated values of σ for surface ages between 1 and 3 ms are narrowly distributed around 0.52 N/m, which compares favorably with the range of 0.50–0.51 N/m reported by Carroll and Warwick (1987) for 60Sn–40Pb solder and temperatures between 210 and 250 °C. Carroll and Warwick used a maximum bubble pressure technique to obtain these values. Hoar and Melford (1957) used a capillary rise technique to obtain values from 0.535 N/m down to 0.520 N/m in the temperature range of 180–230 °C for an alloy containing 61.6% Sn by weight. White (1971) employed a sessile drop technique and obtained values of 0.480–0.485 N/m for a 60.12% Sn alloy in the temperature range of 220–260 °C. Finally, Bellizia et al. (2003) reported a value $\sigma = 0.49$ N/m for solder identical to the one employed in the present work. The excellent agreement between the current values of σ and past measurements for unoxidized solder further validates the present technique, at least when surface properties remain unchanged. For molten solder exposed to higher O_2 atmosphere concentrations, the surface tension is expected to decrease.

According to the data in Table 2, the three higher concentrations (3700 ppm, 1.16%, and 2.03%) seem to contain enough O_2 to be adsorbed on the molten solder surface and reduce σ within the time scales of the experiment. Visual proof of this is demonstrated in Fig. 4, which shows initially identical molten solder jets exposed to varying O_2 concentrations in N_2. The model of Bechtel et al. (1995) indicates that the wavelength of the oscillating jet increases when the surface tension decreases, and vice versa. In Fig. 4(a)–(c), i.e., in low oxygen concentrations, the wavelength remained virtually unchanged, indicating a similar surface tension for all three cases. On the other hand, the wavelengths in Fig. 4(d)–(f) are longer, thus producing lower surface tension values (Table 2). For both 1.16% and 2.03% O_2 concentrations, the surface tension was constant with time, at least for the early surface ages that data is available. In addition, σ for the 1.16% case practically equaled the value in 2.03%. This may be attributed to the rapid formation of an adsorbed oxygen monolayer on the reactive Sn/Pb melt surface. Once the oxygen

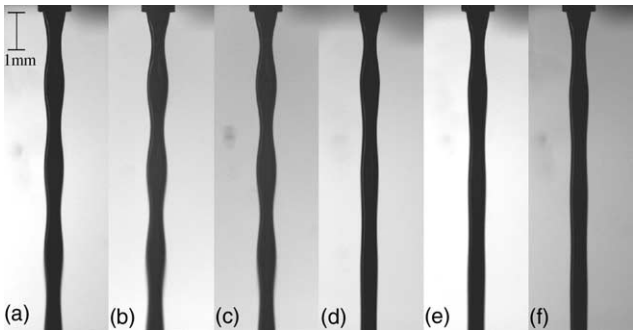

Fig. 4. Molten solder jets ejected in varying O_2 concentrations in N_2; (a) 15 ppm, (b) 103 ppm, (c) 990 ppm, (d) 3700 ppm, (e) 1.16%, (f) 2.03%. All images correspond to views along the minor axis of the elliptical orifice. Length scale shown in (a) applies to all images.

monolayer is formed, the surface tension is not expected to change further with surface age or ambient gas concentration. The formation of this oxygen monolayer, and the induced reduction in surface tension, probably occurred at a surface age below the times measurable with the experimental apparatus, i.e., O(1 ms). Thus the reduced value of σ for concentrations above 1%, if interpreted as caused by oxygen attachment to the melt surface, should represent the surface tension of 63Sn–37Pb containing an adsorbed oxygen monolayer. This, in turn, suggests a characteristic time below 1 ms required for the molten-metal surface to be saturated by adsorbed oxygen at ambient O_2 concentrations of 1% or higher. The kinetic-fluodynamic diagrams for liquid metal-oxygen systems reported in Ricci et al. (1994) allow the estimation of the time required to form an adsorbed oxygen monolayer on the melt surface exposed to an inert carrier flow containing definite amounts of oxygen. For molten tin at 232 °C, this time was reported to be ~44s at 1 ppm O_2 in Helium. If one assumes linearity, the oxygen monolayer formation period at 1000 ppm, 1% and 10% O_2 concentrations would be, respectively, 44, 4.4, 0.4 ms for pure tin. These time scales, as predicted by the analysis of Ricci et al. (1994), appear longer but within an order of magnitude of those designated in the present work. This discrepancy may be due to the presence of nitrogen in the current work (instead of He used in Ricci et al., 1994), or the added presence of Pb in the molten multicomponent phase. It may also be attributed to the inherent differences between the two physical configurations, which affect the gas diffusion layer characteristics above the liquid metal surface, and, in turn, the transport of oxygen molecules to it.

According to the above, the adsorption rates of oxygen on the solder melt surface when exposed to ambient O_2 concentrations as high as 1000 ppm were too slow to be resolved by the present experimental technique, which has the capability to detect changes in the time window 1–3 ms. On the other hand, the corresponding adsorption rates at concentrations over 1% were found to be too fast for the technique. In order to document gradual reduction of surface tension within the time scales resolved in this experiment, an additional case was performed with O_2 concentration between 1000 ppm and 1%. The reduced data for the 3700 ppm case is given in Table 2, and shows a reduction in σ from 0.49 N/m at 1 ms, to 0.40 N/m at 1.6 ms. The higher value of σ corresponds to unoxidized solder, while the lower value is nearly identical to σ in 1% O_2, thus supporting the hypothesis that the oxygen monolayer in a 3700 ppm O_2 ambient atmosphere form within ~1.6 ms. This result also reaffirms the previously stated conclusion that the oxygen monolayer in the 1% O_2 case has already formed at 1 ms. It is worth noting that the reduction in σ cannot be attributed to cooling of the melt with distance from the orifice, as such cooling should also have affected all other cases investigated in this study (Table 2).

As stated in Section 4, the bulk viscosity of the solder melt was assumed to be constant in reducing the surface tension data from the experimental images. The effect of liquid viscosity is to damp out the oscillations of the jet (Bechtel et al., 1995). In other words, an increased bulk viscosity under identical jet ejection conditions would result in less pronounced differences between the major and minor semiaxes at any given location from the orifice. As with surface tension, there appeared to be little change in viscosity for lower O_2 concentrations (see Fig. 4 cases for <1000 ppm). However, increased damping of the jet—indicated by a lessened vibration amplitude—was apparent in the highest three O_2 concentrations; Fig. 4(d)–(f). Again, the 3700 ppm concentration seems to represent the transition from undamped to damped wave amplitudes. This apparent increase in viscosity, which is accompanied by a reduction in surface tension, is most likely caused by the adsorbed oxygen on the jet surface.

In addition to the six O_2 concentrations listed in Table 2, molten solder was also jetted in air. This resulted in the immediate formation of a circular (or near circular) solder jet, as shown in Fig. 5. Note that while the jet in Fig. 5 is shown horizontally, the actual jet orientation during the experiment was vertical. The jet

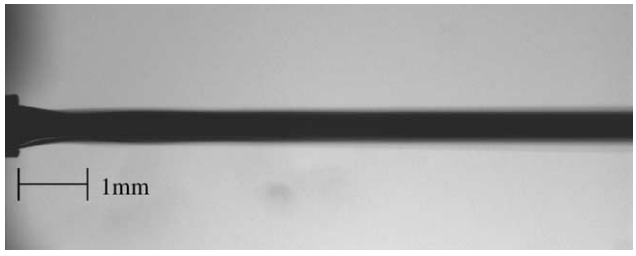

Fig. 5. Molten solder jet issued in air through the elliptical orifice. The actual jet orientation was in the vertical direction.

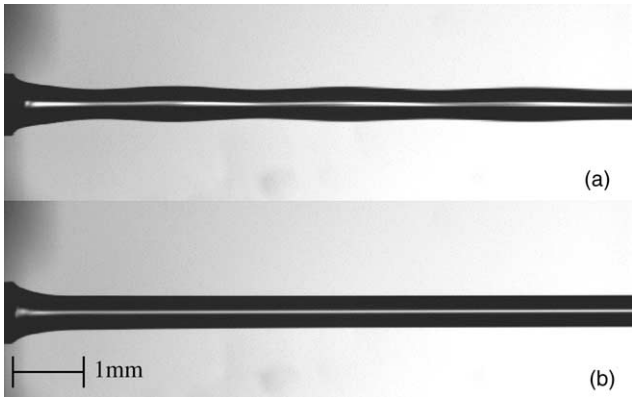

Fig. 6. (a) Pure water jet, (b) water jet containing 10% (volume) liquid detergent. Both jets were issued through the same elliptical orifice. The actual jet orientation was in the vertical direction. Note the rapid establishment of the cylindrical column when the detergent is present in (b).

either becomes circular soon after emerging from the orifice, or the oscillation is too small to measure. In either case, the lack of jet waveform structure did not allow surface tension measurements in air. In order to identify the reasons for this behavior, similar experiments were performed using deionized water, as well as deionized water mixed with significant amounts of liquid detergent. Fig. 6(a) shows a pure deionized water jet issued through the same elliptical nozzle at 1.9 m/s. The water jet displays the expected oscillating shape, similar to that seen in solder. However, when liquid detergent (~10% by volume) is added to the water, the jet rapidly forms a cylindrical column, as shown in Fig. 6(b). Again, while the jets in Fig. 6 are shown horizontally, the experiments were performed with the jets aligned in the vertical direction. The similarity when excessive amounts of oxygen get adsorbed on the melt surface and when high amounts of surfactant are present in the aqueous solution suggests that the lack of waveform structure cannot be attributed to the non-isothermal character of the solder jet. The very rapid transition from elliptical to cylindrical jet geometry could be associated with the degradation of surface tension, but elevated viscosities could also trigger the same behavior by increased dampening. In other words, it is possible that both lower surface tension and higher viscosity combine to cause this behavior. Although the transition from elliptical to circular cross section is not understood at this point, it is clear that the capabilities of the current experimental technique are exceeded when jetting molten solder in air.

It is noted that the images obtained for water jets were considerably sharper than those of molten solder. This is probably due to the non-isothermal conditions in the environmental chamber when jetting solder. The molten solder emerges from the orifice at ~230 °C, while the ambient gas is at ~50 °C. Therefore, the increased blurriness in the solder case is believed to be due to natural convection currents, which introduce additional excitation disturbances to the jet.

8. Kinetic considerations

Dynamic adsorption of oxygen onto liquid metal surfaces can be a complex process, affected by dissolution of oxygen atoms in the bulk of the metal and formation of condensed or volatile oxides. Conditions of surrounding atmosphere temperature and oxygen partial pressure can be defined under which the surface may be saturated or cleaned depending on the relevant thermodynamic properties (Ricci et al., 1998a,b; Ratto et al., 2001). Under conditions relevant to solder jetting, temperatures are relatively low and the high thermodynamic stability of SnO_2 and low solubility of oxygen in bulk lead–tin alloys combine to simplify the process (Otsuka and Kozuka, 1981; Otsuka et al., 1981). Adsorption of oxygen on the liquid metal jet surface occurs by transport of oxygen molecules to surface sites, followed by dissociation to adsorbed atoms. The rate of the overall surface coverage with oxygen would be controlled by the slower of the two processes, either transport or dissociation. Dissociation is a fast reaction, so mass transport is the likely rate-controlling step in the process.

A molten solder jet emerging from a nozzle is expected to have a clean surface (in terms of oxygen) because of the low solubility of oxygen in the melt. Upon emergence of the jet from the orifice, oxygen must be transported to the surface from the gas phase by mass diffusion. The jet usually breaks up in a few ms, therefore, if oxygen transport is too slow to produce substantial coverage in this time scale, then droplet formation is not be affected by oxygen. If oxygen transport is controlled by diffusion in the gas phase, and assuming one-dimensional diffusion of oxygen in nitrogen, then the time required for the surface to become saturated by oxygen is given by (Gaskell, 1992)

$$t = (\Gamma_s/2C_0)^2\pi/D_{O_2\text{–}N_2}. \quad (6)$$

In the above, Γ_s denotes the surface excess of oxygen at saturation (monolayer fully formed), while C_0 is the concentration of oxygen in the gas phase, and $D_{O_2\text{–}N_2}$ is the binary interdiffusion coefficient of oxygen in nitrogen. The concentration C_0 can be calculated under the assumption of ideal gas behavior, while $D_{O_2\text{–}N_2}$ can be determined according to Bird et al. (1960). Eq. (6) shows that the time required to saturate the surface is inversely proportional to the square of the concentration of oxygen in the gas phase. Using the value $C_0 = 0.132$ g mol/m^3 corresponding to 3700 ppm, $D_{O_2\text{–}N_2} = 0.23$

cm^2/s at 318 K (chamber atmosphere), and estimating the value of Γ_s from the atomic radius of the metal (in tin $\Gamma_s \sim 2 \times 10^{-5}$ g mol/m^2), we obtain a *first order* estimate of the saturation time $t \approx 0.8$ ms at the 3700 ppm O_2 concentration. This theoretical estimate is in good agreement with the experimentally determined value of 1.6 ms, for the time required to form an oxygen monolayer over the surface of the reactive solder melt. In turn, this finding supports the hypothesis that mass diffusion is the rate limiting process controlling oxygen adsorption on the solder melt surface.

9. Conclusion

The oscillating jet technique has been used in conjunction with the theoretical model of Bechtel et al. (1995) to convert jet waveforms to dynamic surface tension values as a function of distance from an elliptical orifice (major/minor diameters 664 μm/312 μm). The jetted material is molten eutectic 63%Sn–37%Pb solder, an ultra-pure alloy used in the assembly of microelectronic components. This tin alloy is susceptible to the adsorption of oxygen, which degrades its surface properties even in small quantities. Measurements of surface tension of such melts exposed to oxygen are useful to assist the commercialization of solder jet technology in the manufacturing of microelectronics. The adopted model formulation was based on the assumption that surface tension and viscosity are constant in the same wavelength, although σ is allowed to change between wavelengths (thus producing dependence on the axial coordinate, or likewise surface age). The jet waveforms recorded in the experiments were utilized to deduce the variation of surface tension of the solder melt with distance from the orifice in different O_2/N_2 gas atmospheres. Measurements were performed for oxygen concentrations ranging from 15 ppm to 2.03% (balance N_2), as well as in air. The jet operating conditions corresponded to surface ages in the range 1–3 ms. Solder mass flow rates were around 2.4 g/s (typical), translating into average exit velocities of ~1.8 m/s. The corresponding typical values of the relevant dimensionless groups were $We = 0.16$, $Re = 49$, and $Fr = 165$.

Solder surface tension measurements in low O_2 concentrations (<1000 ppm) resulted in non-oxidized surface tension values of ~0.52 N/m, a value in close agreement with previous studies. The experimental data suggested a characteristic time below 1 ms for the molten-metal surface to be saturated by adsorbed oxygen at ambient O_2 concentrations of 1% or higher. Dynamic surface tension of solder and an apparent increase in melt viscosity were documented at an O_2 concentration of 3700 ppm. For this gas mixture, the time scales of oxygen adsorption onto the solder jet interface were estimated to be ~0.8 ms, based on a simple mass diffusion analysis. This estimate is in good agreement with the experimentally determined time of 1.6 ms for the formation of an oxygen monolayer over the surface of the reactive solder melt. This supports the hypothesis that mass diffusion is the rate limiting process controlling oxygen adsorption on the solder melt surface. The capabilities of the experimental technique were clearly exceeded when jetting in air. Finally, the data produced in this study suggested that the maximum ambient O_2 concentration for reliable solder jetting appears to be ~1000 ppm.

Acknowledgements

This work was supported by NASA grants NAG8-1473 and NGT5-50214. We acknowledge the support of MicroFab Technologies in terms of providing equipment and expertise on the jetting instrumentation. The authors are indebted to Bin Xiong who wrote the computer program solving the inverse problem. Art Sawczuk made contributions to the design of most experimental components, and was responsible for their construction.

References

Bechtel, S.E., Cooper, J.A., Forest, M.G., Petersson, N.A., Reichard, D.L., Saleh, A., Venkataramanan, V., 1995. A new model to determine dynamic surface tension and elongational viscosity using oscillating jet measurements. J. Fluid Mech. 293, 379–403.

Bechtel, S.E., Forest, M.G., Youssef, N.T., Zhou, H., 1998. The effect of dynamic surface tension on the oscillation of slender elliptical Newtonian jets. Trans. ASME J. Appl. Mech. 65, 694–704.

Bellizia, G., Megaridis, C.M., McNallan, M., Wallace, D.B., 2003. A capillary-jet instability method for measuring dynamic surface tension of liquid metals. Proc. R. Soc. London A 459, 2195–2214.

Bird, R.B., Stewart, W.E., Lightfoot, E.N., 1960. Transport Phenomena. John Wiley & Sons, New York.

Bohr, N., 1909. Determination of dynamic surface tension by the method of jet vibration. Philos. Trans. R. Soc. London A 209, 281–317.

Carroll, M.A., Warwick, M.E., 1987. Surface tension of some Sn–Pb alloys: Part I. Effect of Bi, Sb, P, Ag, and Cu on 60Sn–40Pb solder. Mater. Sci. Technol. 3, 1040–1045.

Gaskell, D.R., 1992. An Introduction to Transport Phenomena in Materials Engineering. Macmillan Publishing Co., NY.

Godin, R., 1996. Application of eutectic solder using solder jetting technology. In: Proceedings of the Technical Program of Surface Mount International, September 10–12, San Jose, CA.

Haj-Hariri, H., Poulikakos, D., 2000. Capillary instability of a cylindrical jet with an elastic shroud: a model for the breakup of an oxidized metal jet. Trans. ASME 67, 626–628.

Hayes, D.J., Wallace, D.B., Boldman, M.T., Marusak, R.E., 1993. Picoliter solder droplet dispensing. Int. J. Microcirc. Electron. Packaging 16, 173–180.

Hiller, W.J., Kowalewski, T.A., 1989. Surface tension measurements by the oscillating droplet method. PhysicoChem. Hydrodyn. 11, 103–112.

Hoar, T.P., Melford, D.A., 1957. The surface tension of binary liquid mixtures: lead + tin and lead + indium. Trans. Faraday Soc. 53, 315–326.

Keene, B.J., 1988. Review of data for the surface tension of iron and its binary alloys. Int. Mater. Rev. 33, 1–37.

Munson, B.R., Young, D.F., Okiishi, T.H., 2002. Fundamentals of Fluid Mechanics. John Wiley & Sons, New York.

Otsuka, S., Kozuka, Z., 1981. Further study on the activities of oxygen in liquid Pb and Sb by a modified Coulometric titration method. Metall. Trans. B 12, 616.

Otsuka, S., Sano, T., Kozuka, K., 1981. Activities of oxygen in liquid Bi, Sn, and Ge from electrochemical measurements. Metall. Trans. B 12, 427.

Passerone, A., Ricci, E., Sangiorgi, R., 1990. Influence of oxygen contamination on the surface tension of liquid tin. J. Mater. Sci. 25, 4266–4272.

Ratto, M., Ricci, E., Arato, E., Costa, P., 2001. Oxidation of metals with highly reactive vapors: Extension of Wagner theory. Metall. Mater. Trans. B 32, 903–911.

Rayleigh, L., 1879. On the capillary phenomena of jets. Proc. R. Soc. London 29, 71–97.

Rayleigh, L., 1890. On the tension of recently formed surfaces. Proc. R. Soc. London 41, 281–287.

Reichard, D.L., Cooper, J.A., Bechtel, S.E., Fox, R.D., 1997. A system for determining dynamic surface tension using the oscillating jet technique. Atomization Sprays 7, 219–233.

Ricci, E., Passerone, A., Castello, P., Costa, P., 1994. Surface reactivity of liquid metal with oxygen and its relationship with surface tension measurements: a kinetic-fluodynamic model. J. Mater. Sci. 29, 1833–1846.

Ricci, E., Nanni, L., Arato, E., Costa, P., 1998a. Characteristic times of oxygen mass transfer at the liquid metal–vapour interface. J. Mater. Sci. 33, 305–312.

Ricci, E., Nanni, N., Passerone, A., 1998b. Oxygen transport and dynamic surface tension of liquid metals. Philos. Trans. R. Soc. London A 356, 857–869.

Ronay, M., 1978a. Determination of the dynamic surface tension of inks from the capillary instability of jets. J. Colloid Interface Sci. 66, 55–67.

Ronay, M., 1978b. Determination of the dynamic surface tension of liquids from the instability of excited capillary jets and from the oscillation frequency of drops issued from such jets. Proc. R. Soc. London 361, 181–206.

Shavit, U., Chigier, N., 1995. The role of dynamic surface tension in air assist atomization. Phys. Fluids 7, 24–33.

Wallace, D.B., 1993. Capillary instability of a jet of liquid metal. ASME J. Fluids Eng. 115, 529–532.

White, D.W.G., 1971. The surface tensions of Pb, Sn, and Pb–Sn alloys. Metall. Trans. 2, 3067–3071.

Xiong, B., Megaridis, C.M., Poulikakos, D., Hoang, H., 1998. An investigation of key factors affecting solder microdroplet deposition. J. Heat Transfer 120, 259–270.